npg

ORIGINAL ARTICLE

Multifaceted roles of *miR-1*s in repressing the fetal gene program in the heart

Yusheng Wei[1, 5, *], Siwu Peng[1, *], Meng Wu[1], Ravi Sachidanandam[2], Zhidong Tu[2], Shihong Zhang[3], Christine Falce[4], Eric A Sobie[4], Djamel Lebeche[3], Yong Zhao[1]

[1]Mindich Child Health and Development Institute, Department of Genetics and Genomic Sciences, Icahn School of Medicine at Mount Sinai, One Gustave L. Levy Place, Box 1040, New York, NY 10029, USA; [2]Institute for Genomics and Multiscale Biology, Icahn School of Medicine at Mount Sinai, One Gustave L. Levy Place, New York, NY 10029, USA; [3]Cardiovascular Institute, Icahn School of Medicine at Mount Sinai, One Gustave L. Levy Place, New York, NY 10029, USA; [4]Pharmacology and Systems Therapeutics, Icahn School of Medicine at Mount Sinai, One Gustave L. Levy Place, New York, NY 10029, USA

miRNAs are an important class of regulators that play roles in cellular homeostasis and disease. Muscle-specific miRNAs, *miR-1-1* and *miR-1-2*, have been found to play important roles in regulating cell proliferation and cardiac function. Redundancy between *miR-1-1* and *miR-1-2* has previously impeded a full understanding of their roles *in vivo*. To determine how miR-1s regulate cardiac function *in vivo*, we generated mice lacking *miR-1-1* and *miR-1-2* without affecting nearby genes. *miR-1* double knockout (*miR-1* dKO) mice were viable and not significantly different from wild-type controls at postnatal day 2.5. Thereafter, all *miR-1* dKO mice developed dilated cardiomyopathy (DCM) and died before P17. Massively parallel sequencing showed that a large portion of upregulated genes after deletion of *miR-1*s is associated with the cardiac fetal gene program including cell proliferation, glycolysis, glycogenesis, and fetal sarcomere-associated genes. Consistent with gene profiling, glycogen content and glycolytic rates were significantly increased in *miR-1* dKO mice. *Estrogen-related Receptor β* (*Errβ*) was identified as a direct target of *miR-1*, which can regulate glycolysis, glycogenesis, and the expression of sarcomeric proteins. Cardiac-specific overexpression of *Errβ* led to glycogen storage, cardiac dilation, and sudden cardiac death around 3-4 weeks of age. We conclude that *miR-1* and its primary target *Errβ* act together to regulate the transition from prenatal to neonatal stages by repressing the cardiac fetal gene program. Loss of this regulation leads to a neonatal DCM.

Keywords: *miR-1-1*; *miR-1-2*; fetal gene program; dilated cardiomyopathy
Cell Research (2014) **24**:278-292. doi:10.1038/cr.2014.12; published online 31 January 2014

Introduction

The heart adapts and generates a cardiac output to match the body's circulatory demands during fetal and postnatal life by employing different circulations, energy use, and myocardial sarcomeric proteins. For a successful transition from the fetal to postnatal stages, the heart represses the fetal gene program and activates an adult genetic program, by which it increases cardiac contractility and alters energy metabolism [1, 2].

The fetal heart expresses a distinct set of sarcomere-associated genes, which share molecular signature with skeletal muscle and smooth muscle. For example, *Acta1* (*actin, alpha 1, skeletal muscle*) predominates in the fetal and neonatal human heart, whereas *Actc1* (*actin, alpha, cardiac muscle 1*) is the predominant form in adult heart [3]. Fetal heart but not adult heart also expresses *Acta2* (*smooth muscle α-actin*), *Tagln* (or *Sm22*), *Cnn1* (*calponin-1*), *Cnn2* (*calponin-2*), *Crp2* (*cysteine- and glycine-rich protein 2*), and *Myl6*, which are specifically expressed in smooth muscle later on [4-9]. The fetal heart also expresses cardiac-specific sarcomeric proteins such as βMhc, while αMhc is the adult isoform. Upon full

cardiac maturation, these genes are no longer expressed in the adult heart. Under pathophyiologic conditions, the heart reactivates the fetal gene program including many of the fetal sarcomere-associated genes, such as *Acta1*, *Acta2*, and *βMhc* [10].

Cardiac contractile performance is tightly coupled to energy metabolism. During fetal life when mitochondrial oxidation is less developed, the developing heart relies predominantly on glycolysis to generate the bulk of its ATP. Glucose is stored as glycogen, which comprises ~35% of the weight of fetal cardiomyocytes and serves as substrate reservoir. After birth, the heart switches from glycolysis to the β-oxidation of fatty acids as the major ATP source, and glycogen content decreases to 4% in adult cardiomyocytes [11]. Proper regulation of energy metabolism is critical for cardiac structural and functional support. Despite glycogen being essential for cardiac development [12] and glycogen storage being a common feature of certain types of cardiomyopathy [13, 14], the genetic regulation of glycolysis and glycogenesis in the fetal heart remains completely unknown.

A well-coordinated switch in sarcomeric proteins and energy metabolism during the transition from prenatal to neonatal stages is critical for proper cardiac function. Emerging evidence suggests that nuclear receptors may regulate this transition. First, in the mammalian heart, the nuclear receptors PPAR family and Estrogen-related receptor γ (ERRγ) activate genes involved in mitochondrial β-oxidation and oxidative metabolism in adult heart [15, 16]. Second, dERR, the only ERR ortholog in *Drosophila*, directs glucose metabolism during larval development. *dERR* mutants die due to defects in glycolysis and other aspects of carbohydrate metabolism [17]. Third, nuclear receptors have been shown to regulate the muscle fiber program in skeletal muscle, raising the possibility that these nuclear receptors may regulate sarcomeric genes in the heart as well [18].

We focus on miRNAs, a class of genetic regulators that play key roles in cellular homeostasis and disease [19-22]. Among all miRNAs identified, *miR-1* is one of the most evolutionarily conserved. In all vertebrates, there are two *miR-1*s, *miR-1-1* and *miR-1-2*, which are clustered with *miR-133a2* and *miR-133a1*, respectively, on separate chromosomes. *miR-1* has been shown to play important roles in regulating cardiac rhythm and skeletal muscle proliferation [23-29]. Deletion of *miR-133a-1* and *miR-133a-2* results in failure to suppress numerous fetal sarcomere-associated genes in the neonatal heart, which are generally not expressed in the adult heart but become specifically expressed in the smooth muscle. While these data demonstrate that *miR-133a-1* and *miR-133a-2* repress one aspect of the cardiac fetal gene pro-

gram, how *miR-1*s exactly regulate cardiac function *in vivo* is not clear. Mouse models that specifically delete *miR-1*s without affecting nearby genes are essential to address the role of *miR-1*s *in vivo*. In this study, we generated mice specifically lacking both *miR-1-1* and *miR-1-2*. This revealed a surprisingly multifaceted role of *miR-1*s in postnatal repression of the fetal cardiac gene program.

Results

Targeted deletion of miR-1-1 and miR-1-2 in mice

miR-1-1/miR-133a-2 and *miR-1-2/miR-133a-1* clusters are located on chromosome 2 and in an intron of the *Mind Bomb 1* (*Mib1*) gene on chromosome 18, respectively (Figure 1A). Mature forms of *miR-1-1* and *miR-1-2* are identical. Using primers specifically detecting precursors of *miR-1-1* and *miR-1-2*, we found that the expression of *miR-1-1* and *miR-1-2* increases as the heart develops, reaching peak levels perinatally (Figure 1B). The dynamic expression implies critical roles of *miR-1-1* and *miR-1-2* in neonates.

To uncover the functions of both *miR-1-1* and *miR-1-2*, we generated conditional alleles at both loci. The *miR-1-1* floxed allele (*miR-1-1$^{f/f}$*) was created by inserting two loxP sites flanking a 0.4 kb genomic region encompassing the *miR-1-1* precursor (Figure 1C). A similar strategy was used to generate *miR-1-2* floxed allele (*miR-1-2$^{f/f}$*) in which two loxP sites flank a 0.26 kb genomic region (Figure 1C). Targeted ES cells were identified by Southern blot (Figure 1D). The neomycin cassette flanked by Frt sites was excised by breeding *miR-1-1$^{f/f}$* and *miR-1-2$^{f/f}$* mice with FLPe mice. *miR-1-1$^{f/f}$* or *miR-1-2$^{f/f}$* mice were phenotypically normal, suggesting that insertion of loxP sites did not affect transcription or processing of the primary *miR-1* transcripts. Germline deletion of *miR-1* was achieved by breeding *miR-1* floxed alleles with *Prm-Cre* mice (Supplementary information, Figure S1A).

Complete deletion of *miR-1*s by Cre-mediated recombination with Prm-Cre was confirmed by RT-PCR (Supplementary information, Figure S1B). Importantly, neither expression of *miR-133*s nor the splicing pattern of the *Mib* transcript was affected in *miR-1-1/miR-1-2* double knockout mice (*miR-1-1$^{-/-}$*;*miR-1-2$^{-/-}$*; henceforth referred to as *miR-1 dKO*) as assessed by quantitative PCR (qPCR) (Supplementary information, Figure S1C and S1D). Thus, the phenotypes observed in *miR-1 dKO* mice were attributed to the specific loss of *miR-1*s.

Deletion of miR-1s causes dilated cardiomyopathy and postnatal lethality

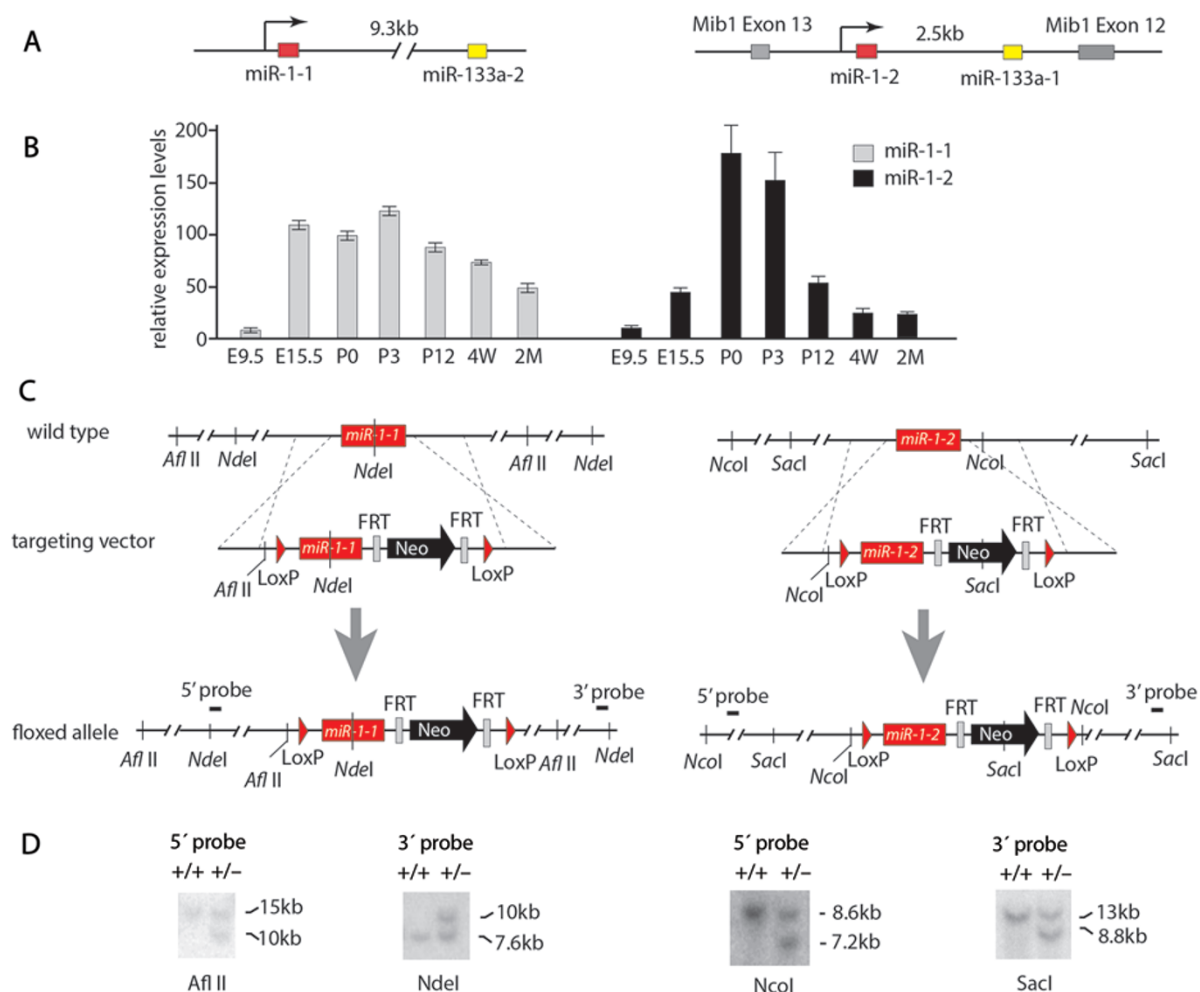In contrast to previous reports of partially penetrant

Figure 1 Targeted deletion of *miR-1-1* and *miR-1-2 in vivo*. **(A)** *miR-1-1/miR-133a-2* and *miR-1-2/miR-133a-1* clusters are on separate chromosomes. **(B)** Dynamic expression of *miR-1-1* and *miR-1-2* in the heart during developmental stages to adult. The expression level of 18S RNA was used for normalization (Ct18). Relative transcript levels of *miR-1* were determined after arbitrarily designating Ct38 as 1. E, embryonic; W, week; M, month. **(C)** Targeting strategies to generate *miR-1-1* and *miR-1-2* knockout mice. **(D)** Targeted ES cells were identified by Southern blot using 5′ and 3′ probes.

embryonic lethality in *miR-1-2* mutants, we found that deletion of either *miR-1-1* or *miR-1-2* did not cause embryonic lethality (Supplementary information, Tables S1 and S2). *miR-1-1* and *miR-1-2* single knockout mice were viable. The discrepancy is likely due to effects of residual LacZ and neo cassettes present in the mutant *miR-1-2* locus in the previous study [23]. Histologic examination did not reveal congenital heart defects such as atrial septal defect or ventricular septal defect in *miR-1-1* null, *miR-1-2* null, or *miR-1* dKO mice. Detailed phenotypic characterization of *miR-1-1* or *miR-1-2* single knockout mice is provided in Supplementary information, Figure S2 and Tables S1-S2.

miR-1 dKO pups were viable at birth, and their body sizes were not significantly different from that of wild-type (WT) control at postnatal day 2.5 (P2.5) (Supplementary information, Figure S3A and Table S3). During the first postnatal week, *miR-1 dKO* mice became visibly weak and all died prior to P17 (Figure 2A). Histologic examination revealed no significant difference in heart size between WT and *miR-1 dKOs* at P2.5 (Figure 2B). By P12, the size of *miR-1 dKO* mice was noticeably smaller than that of WT controls (Supplementary information, Figure S3B). Heart-to-body weight (HW/BW) ratio was increased in *miR-1 dKOs* compared with WT controls (Figure 2D). Thereafter, both ventricular chambers of *miR-1 dKO* mice began to dilate, suggesting that severely impaired cardiac function was the cause of death (Figure 2C, top and middle panels). Collagen content was slightly increased in the *miR-1 dKO* hearts
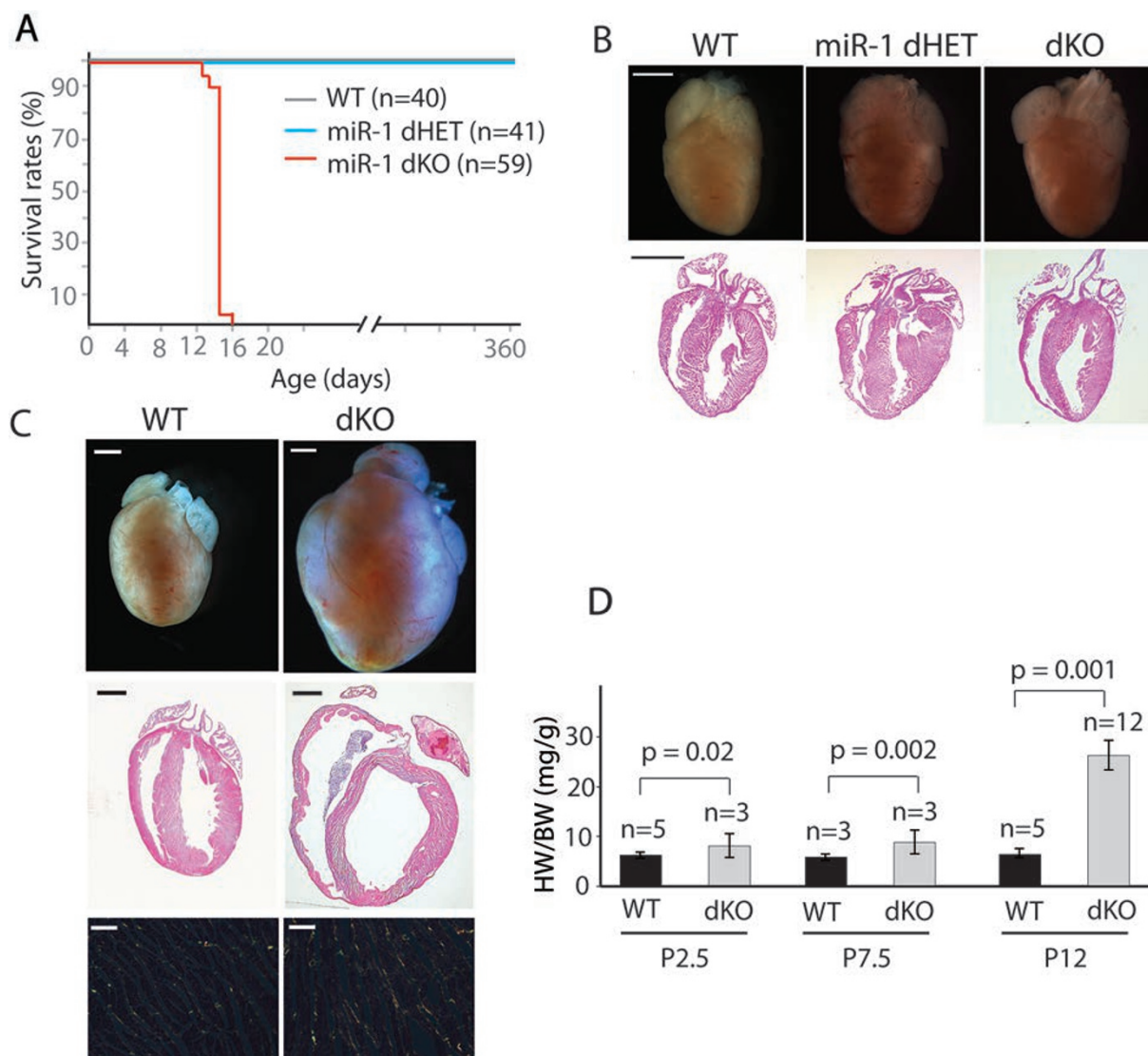
Figure 2 Deletion of *miR-1-1* and *miR-1-2* causes DCM. **(A)** Survival curves of WT, *miR-1-1*$^{+/-}$/*miR-1-2*$^{+/-}$ (*miR-1 dHET*), and *miR-1 dKO* mice. *miR-1 dKO* mice died between P12 and P17. **(B)** The gross morphology and H&E sections of hearts from WT, dHET, and *miR-1 dKO* at P2.5. Scale bar, 1 mm. **(C)** The gross morphology and H&E sections of hearts from WT and *miR-1 dKO* at P12 (top and middle panels). Scale bar, 1 mm. Collagen fibers (bright yellow or orange) were shown by picro-sirius red staining (bottom panel). Scale bar, 50 μm. WT, wild type; *dKO*, double knockout. **(D)** Heart-to-body weight ratio was calculated in *miR-1 dKO*, and was compared with WT at various stages.

as assessed by picrosirius red staining viewed with polarized light (Figure 2C, bottom panel).

Previous studies showed that *miR-1* represses cardiomyocyte proliferation [23, 24]. Consistent with this observation, we found numerous proliferating cardiomyocytes in the *miR-1 dKO* mice at P2.5 and at P7.5 as assessed by anti-phospho-Histone H3 (Ser10) (PH3), a marker for mitotic nuclei in prophase (Figure 3A, 3B and Supplementary information, Figure S4) [30]. As a result, the number of cardiomyocytes was significantly

increased in *miR-1 dKO* mice compared with WT controls (Figure 3C), although the size of cardiomyocytes was slightly smaller in *miR-1 dKO* mice at P2.5 compared with WT controls (Figure 3D and Supplementary information, Figure S5). Thus, we concluded that the increased cardiac mass in the *miR-1 dKO* mice is due to an increase in cardiomyocyte number, not cell size.

Cardiomyocyte apoptosis often accompanies left ventricular dysfunction and remodeling associated with dilated cardiomyopathy (DCM) [31]. To evaluate wheth-
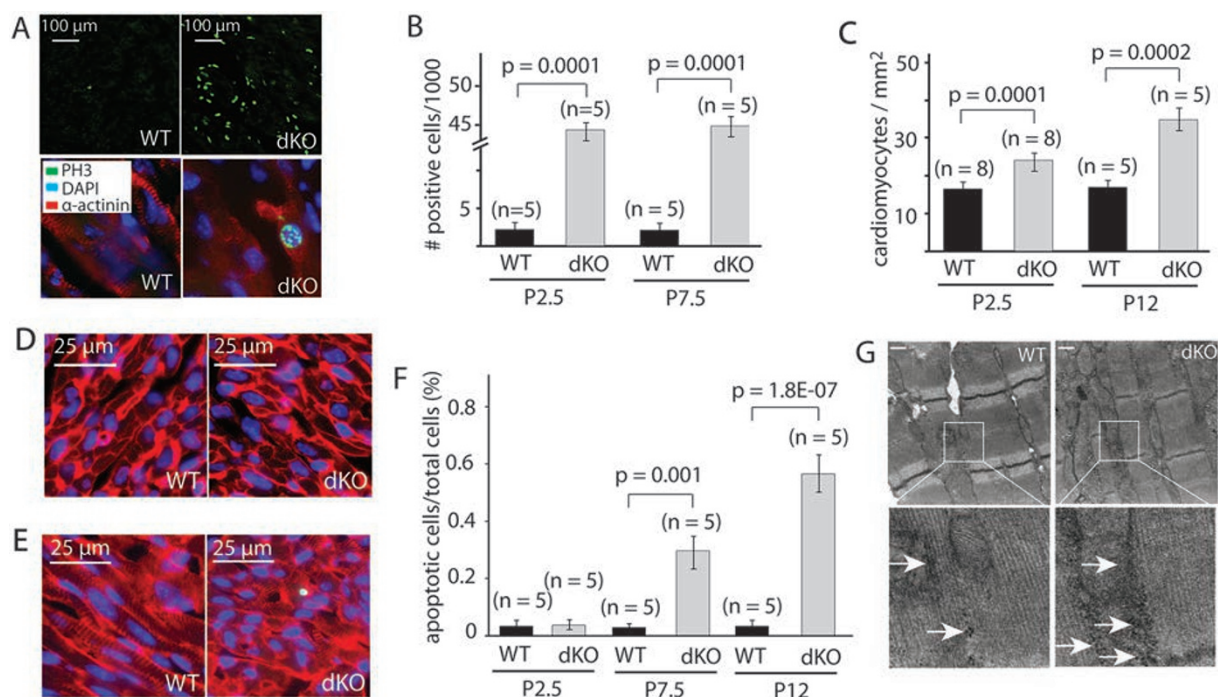
Figure 3 Cellular events after deletion of *miR-1-1* and *miR-1-2*. **(A)** Sections of P2.5 hearts showing proliferating cardiomyocytes as assessed by PH3 staining (green, top panels). High magnification picture (bottom panels) confirming colocalization of PH3 and DAPI signals (blue) in the nucleus of a cardiomyocyte (anti-α-actinin, red). **(B)** Quantification of PH3-positive cardiomyocytes. **(C)** The number of cardiomyocytes in WT and *miR-1 dKO* mice. **(D)** Paraffin sections of the left ventricles at P2.5 stained with wheat germ agglutinin showing cardiomyocyte cross-sectional area. Blue, DAPI staining. **(E)** Cardiomyocyte apoptosis in the heart at P12 was assessed by TUNEL assay (green). Blue, DAPI staining, Red, anti-α-actinin staining. **(F)** Quantification of apoptotic cardiomyocytes of *miR-1 dKO* mice at various stages. **(G)** TEM of hearts from WT and *miR-1 dKO* mice at P12. Glycogen β particles (white arrow) are detected along sarcomeres in cardiomyocytes. Scale bar, 1 μm.

er this is the case in *miR-1 dKO* heart, we performed terminal deoxynucleotidyl transferase dUTP nick end labeling (TUNEL) assays. Prior to the onset of cardiac dysfunction at P2.5, no apoptotic cells were seen in the hearts of *miR-1 dKO* mice or WT controls, suggesting that apoptosis was not a primary cause of cardiac dilation in *miR-1 dKO* mice. At P7.5 and P12, the number of apoptotic cells was increased in the hearts of *miR-1 dKO* mice (Figure 3E and 3F), suggesting that apoptosis may contribute to cardiac decompensation and worsening heart function prior to death. In contrast, Evans blue dye assay revealed no necrosis in hearts of *miR-1 dKO* at P12 (Supplementary information, Figure S6).

Next, we considered the possible existence of ultrastructural lesions in the *miR-1 dKO* heart. Using transmission electron microscopy (TEM), we observed that the sarcomeres, the distribution and structures of mitochondria, and the intercellular junctions in the cardiomyocytes of the *miR-1 dKO* mice were normal at E15.5 and P2.5 (Supplementary information, Figure S7). After the onset of DCM at P12, the edges of Z, I, and A bands

were not as sharp in the *miR-1 dKO* hearts as in WT controls (Figure 3G, top panels). Of note, glycogen β particles, which were sparsely distributed throughout the sarcoplasm of control cardiomyocytes, were strikingly increased, particularly between the sarcomeres, in *miR-1 dKO* hearts (Figure 3G, bottom panels).

To examine whether cardiac dilation observed in the *miR-1 dKO* mice was associated with systolic dysfunction, we performed two-dimensional M-mode echocardiography at P12. Ejection fraction (EF) and fractional shortening (FS), two indices of left ventricular systolic function, were decreased by more than two-thirds (Figure 4A and 4B). Consistent with our histological findings, left ventricular internal dimensions and volumes were significantly increased in the *miR-1 dKO* mice (Figure 4A and 4B). Thus, we concluded that the *miR-1 dKO* mice suffer DCM.

miR-1s repress a fetal gene program

To explore the primary cause of DCM in *miR-1 dKO* mice, we set out to identify differentially expressed
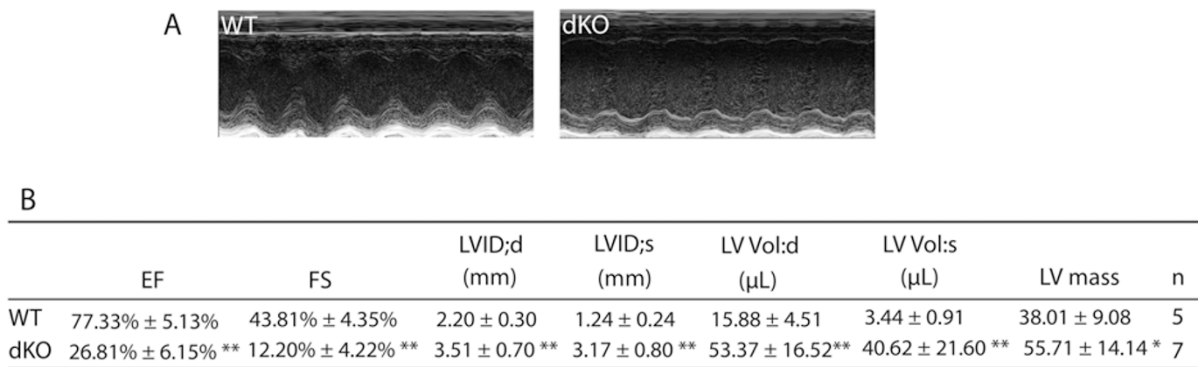
Figure 4 Assessment of left ventricle systolic function by echocardiography. **(A)** M-mode echo to compare LV contraction of the heart from *miR-1 dKO* at P12 to that of WT. **(B)** Quantification of LV function. EF, ejection fraction; FS, fractional shortening; LVID, left ventricular internal diameter; LV Vol, left ventricular volume; LV mass, left ventricular mass; d, end diastolic; s, end systolic. *$P < 0.05$; **$P < 0.01$.

	EF	FS	LVID;d (mm)	LVID;s (mm)	LV Vol:d (µL)	LV Vol:s (µL)	LV mass	n
WT	77.33% ± 5.13%	43.81% ± 4.35%	2.20 ± 0.30	1.24 ± 0.24	15.88 ± 4.51	3.44 ± 0.91	38.01 ± 9.08	5
dKO	26.81% ± 6.15% **	12.20% ± 4.22% **	3.51 ± 0.70 **	3.17 ± 0.80 **	53.37 ± 16.52**	40.62 ± 21.60 **	55.71 ± 14.14 *	7

genes using massively parallel sequencing (mRNA-seq). To avoid secondary effects of cardiac dysfunction on gene expression, we examined the transcriptome at P2.5, when *miR-1 dKO* hearts were morphologically normal. In this manner, hundreds of dysregulated transcripts including previously validated targets of *miR-1* such as *Hand2*, *Irx5*, and *Cx43* were identified (Supplementary information, Table S4) [23-25]. Seed matches are significantly enriched in the 3′ UTR of the upregulated genes, consistent with the critical role of miRNA seed region in recognizing/binding 3′ UTRs of mRNAs (Figure 5A) [23].

Computational analysis revealed that a large portion of the upregulated genes in mutant is associated with the cardiac fetal gene program, i.e., genes associated with fetal mode of metabolism (predominance of glycolysis and glycogenesis) and fetal sarcomeric proteins. Representative candidates from mRNA-seq were further validated by qPCR. For instance, the transcripts of *Pdk3*, a strong inhibitor of pyruvate oxidation, were increased in *miR-1 dKO* mice (Figure 5B and 5C). The transcript levels of many genes associated with cell proliferation (e.g., *Hand1/2*) and cell cycle were also significantly increased, consistent with the cardiac hyperplasia observed after loss of *miR-1*s (Supplementary information, Table S4).

If *miR-1*s repress the fetal gene program, we would expect the fetal genes to increase during the embryonic stage following the loss of *miR-1*s. To test this, we performed mRNA-seq using hearts from *miR-1 dKOs* and WT controls at E15.5. Many fetal transcripts (such as *Gyg*, *Gbe1*, *Acta2*, *Myh7*, and *Myl9*) were indeed increased at E15.5 after deletion of *miR-1*s (Supplementary information, Table S5). Among the genes that were dys-

regulated at both E15.5 and P2.5, most of them showed similar trend of alterations at these two stages, providing additional evidence that *miR-1*s repress the fetal gene program (Supplementary information, Figure S8).

To further determine whether *miR-1* actively represses the fetal gene program, we overexpressed *miR-1* in the neonatal rat cardiomyocytes via adenoviral transduction. Overexpression of *miR-1* decreased genes that were upregulated in *miR-1 dKO* mice (Figure 5D).

Having established *miR-1* as a repressor of the fetal gene program at the gene expression level, we then decided to determine whether intramyocardial glycogen content and the rate of glycolysis were affected in *miR-1 dKO* mice. As shown in Figure 6A, cardiac glycogen content in both normal and *miR-1 dKO* mice decreased progressively from embryonic life through early postnatal life. However, cardiac glycogen levels were increased by ~2-fold in the *miR-1 dKO* mice compared to WT controls at all stages examined (Figure 6A). Periodic acid-Schiff (PAS) staining further confirmed that a larger amount of carbohydrate macromolecules (presumably glycogen) were present in the hearts from *miR-1 dKO* mice compared to WT controls at all three stages examined (Figure 6B). To determine whether *miR-1*s repress glycolysis, we adapted an established method to determine glycolytic rate in cultured P2.5 neonatal cardiomyocytes [32]. The glycolytic rate was increased in mutant compared with WT controls (Figure 6C). Triglycerides and fatty acids are the main energy substrates in the mature heart. Neither neutral lipid level nor the number of mitochondria was changed in *miR-1 dKO* mice (Figure 6D and 6E), suggesting that loss of *miR-1*s specifically targets the fetal gene profile.

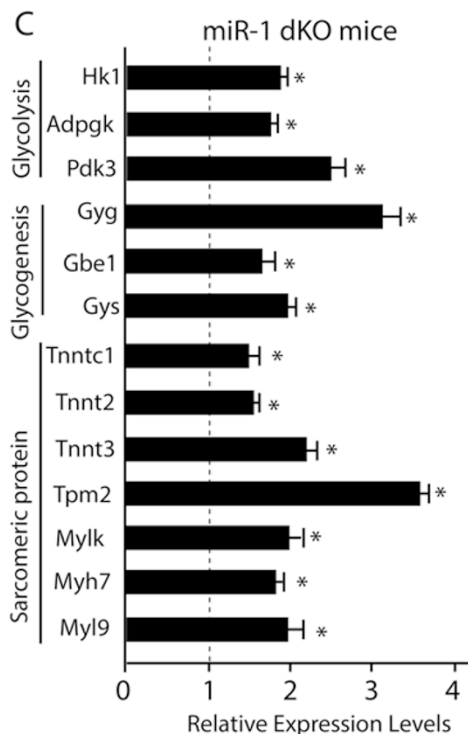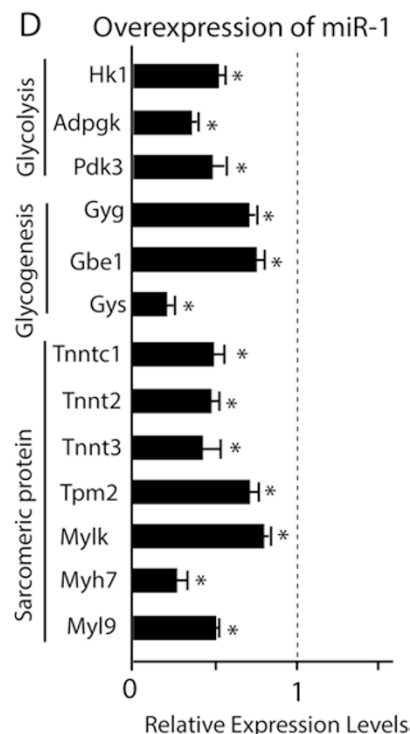Taken together, we concluded that *miR-1*s specifically

Figure 5 *miR-1* suppresses a fetal gene program. **(A)** *miR-1* seed occurrence in 3′ UTR of all mRNAs in mice compared to genes whose transcripts were increased or decreased at E15.5 and P2.5. **(B)** List of genes with increased transcripts involved in glycolysis, glycogenesis, and sarcomere in the heart from *miR-1 dKO* at P2.5 as identified by massively parallel sequencing. **(C)** qPCR validated relative expression levels of most of genes in **B** (*n* = 3, compared to WT). *P < 0.05. **(D)** Overexpression of *miR-1* represses fetal genes in neonatal rat cardiomyocytes (*n* = 3). *P < 0.05.

repress the fetal gene program including glycolysis, glycogenesis, and sarcomeric proteins.

miR-1 directly represses the expression of Errβ, a principal regulator of glycolysis and glycogenesis

Next, we wanted to determine how *miR-1* regulates the fetal gene program. microRNAs are believed to generally bind to 3′ UTR through canonical Watson-Crick base pairing, although there are numerous exceptions [23]. Some fetal genes with *miR-1* canonical binding sites in 3′ UTRs are likely to be direct targets. Representative candidates with *miR-1* binding sites in 3′ UTRs from each category were indeed validated as direct targets of *miR-1* (Supplementary information, Figure S9). However, *miR-1* is unlikely to repress most of fetal genes directly as most of those genes do not have canonical *miR-1* binding sites in their 3′ UTRs.

The genetic regulation of glucose metabolism in the developing heart is completely unknown. To determine the primary transcriptional regulatory circuits controlling fetal sarcomere-associated genes and, particularly glucose metabolism, we examined mRNA-seq data at E15.5 for potential candidate genes that were already upregulated. Serum response factor (Srf) and its co-activator myocardin are transcriptional activators for *miR-1*s and they regulate sarcomere-associated genes [24, 33, 34]. However, they were not attractive candidates as the transcript levels of Srf and myocardin were not increased in
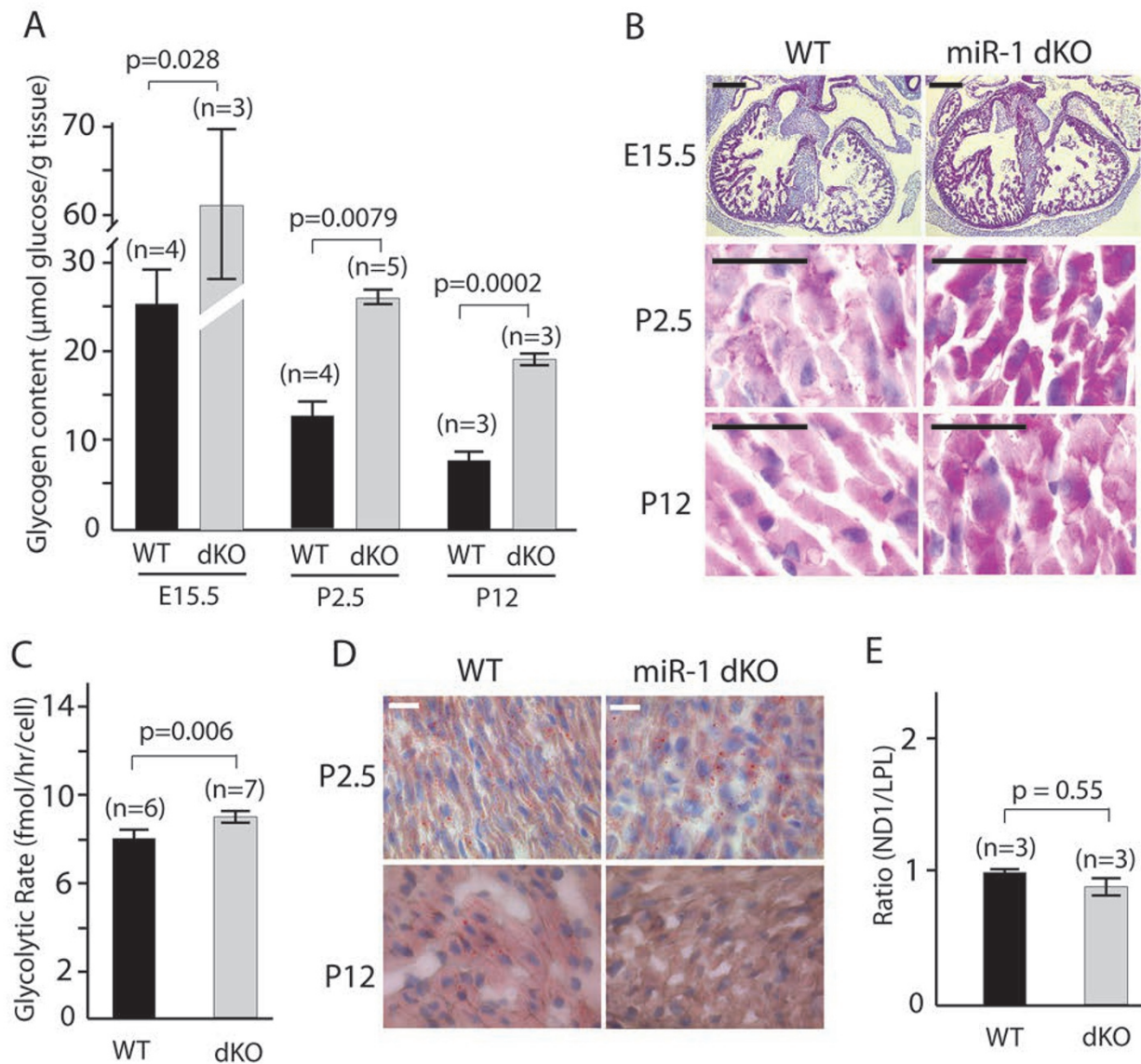
Figure 6 Increased glycolysis and glycogenesis after loss of *miR-1*. **(A)** Glycogen levels were measured in hearts from E15.5 to P12 from WT and *miR-1 dKO* mice. Results were presented as glucose released from glycogen and normalized to tissue weight. **(B)** Comparative PAS staining of carbohydrates (including glycogen) that react with Schiff reagent, resulting in intense pink in hearts from *miR-1 dKO* mice compared to WT (*n* = 3 at each stage). Scale bar, 20 μm. **(C)** Glycolytic rate was expressed as the amount of glucose in fmol converted to pyruvate per hour for each cardiomyocyte. **(D)** Distribution of neutral lipids (red dots) in heart of *miR-1 dKO* mice and in heart of WT at P2.5 and P12 (*n* = 3 at each stage). Scale bar, 10 μm. **(E)** mtDNA quantification. Ratio of ND1 (NADH dehydrogenase subunit 1, which is encoded in mitochondrial DNA) against LPL (lipoprotein lipase, which is encoded in nuclear genome) was used to determine possible change in number of mitochondria.

the *miR-1 dKO* mice (Supplementary information, Table S5).

Nuclear receptors have emerged as candidate regulators of muscle fiber program and energy metabolism. A thorough examination of our mRNA-seq data revealed that the transcript level of e*strogen-related receptor β* (*Errβ*) was consistently increased in *miR-1 dKO* mice in developing and postnatal hearts compared with WT, but transcripts of nuclear receptors PPAR family, Rxra, and thyroid hormone receptor α/β showed no change, suggesting that Errβ could be the primary regulator associated with glycolysis, glycogenesis, and sarcomere-associated genes.

The function of nuclear receptor ERRs is cell context

dependent. The endogenous ligands for Errβ remain unknown and thus it belongs to orphan nuclear receptor family. Errβ regulates muscle fiber-type program in skeletal muscle but its role in heart remains unclear [18]. The expression of *Errβ* was increased at the transcript and protein levels in *miR-1 dKO* mice as assessed by qPCR and western blot, respectively (Figure 7A and 7B). Sequence analysis identified two putative binding sites of *miR-1* in the 3′ UTR of *Errβ* (Figure 7C). To explore

whether *Errβ* is a direct target of *miR-1*, we subcloned its 2.6-kb 3′ UTR into a luciferase reporter. The addition of *miR-1* dramatically repressed the luciferase activity while mutant *miR-1* did not have any effect (Figure 7D), demonstrating that its 3′ UTR is subject to *miR-1* seed-mediated repression *in vivo*. If *Errβ* is a direct target of *miR-1*, its transcript would be expected to decrease when *miR-1* is overexpressed. Indeed, overexpression of *miR-1* in neonatal rat cardiomyocytes reduced Errβ at mRNA
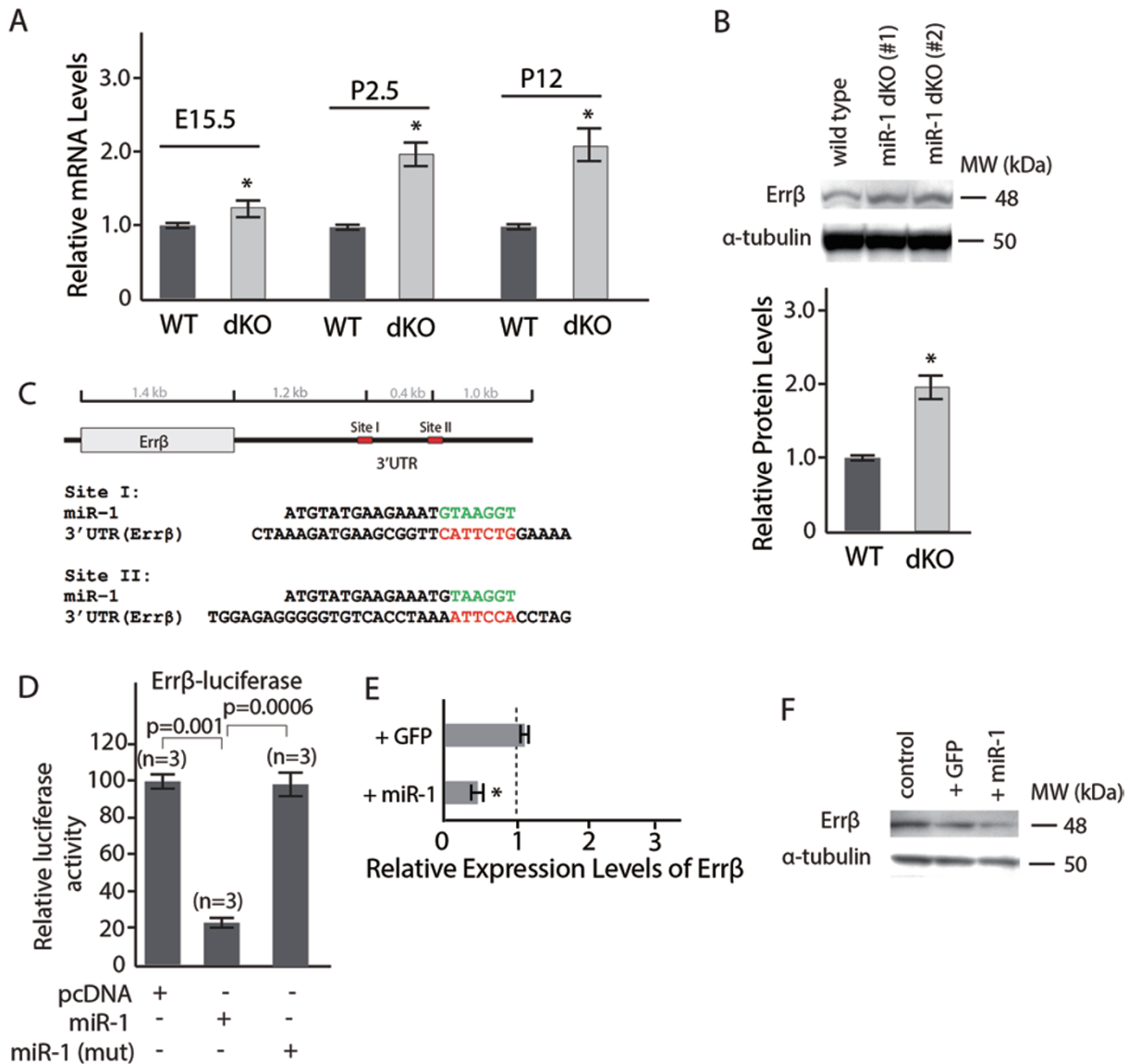

Figure 7 *Errβ* is a direct target of *miR-1*. **(A)** qPCR validated expression of *Errβ* in *miR-1 dKO* mice at three stages (*n* = 3). *P < 0.05. **(B)** Western blot analysis of Errβ in the whole heart lysate from WT and *miR-1 dKO* at P2.5 (*n* = 3) (top). Quantification by densitometry (bottom). **(C)** The 3′ UTR of *Errβ* contains two putative binding sites of *miR-1*. **(D)** The luciferase activity of *Errβ*-luciferase reporter with transfection of *miR-1* or mutant *miR-1*. **(E)** Expression levels of *Errβ* in neonatal rat cardiomyocytes as assessed by qPCR after overexpression of *miR-1* or GFP (*n* = 3). *P < 0.05. **(F)** Protein level of Errβ in neonatal rat cardiomyocytes as assessed by western blot after overexpression of *miR-1* (*n* = 3).

and protein levels (Figure 7E and 7F).

As *Errβ* was identified as a direct target of *miR-1*, we next asked whether it regulates glycolysis and glycogenesis. Robust PAS signal was detected upon overexpression of *Errβ* compared with control (Figure 8A). Glycolytic rate was also significantly increased upon overexpression of *Errβ* (Figure 8B). Numerous fetal genes that were upregulated in *miR-1 dKO* mice were activated upon overexpression of *Errβ* in neonatal rat cardiomyocytes via adenoviral transduction (Figure 8C), suggesting that *Errβ* is the primary downstream executor of *miR-1*. To further confirm whether overexpression of *Errβ* could increase glycogen level *in vivo*, we generated transgenic mice overexpressing *Errβ* in the heart. PAS staining con-
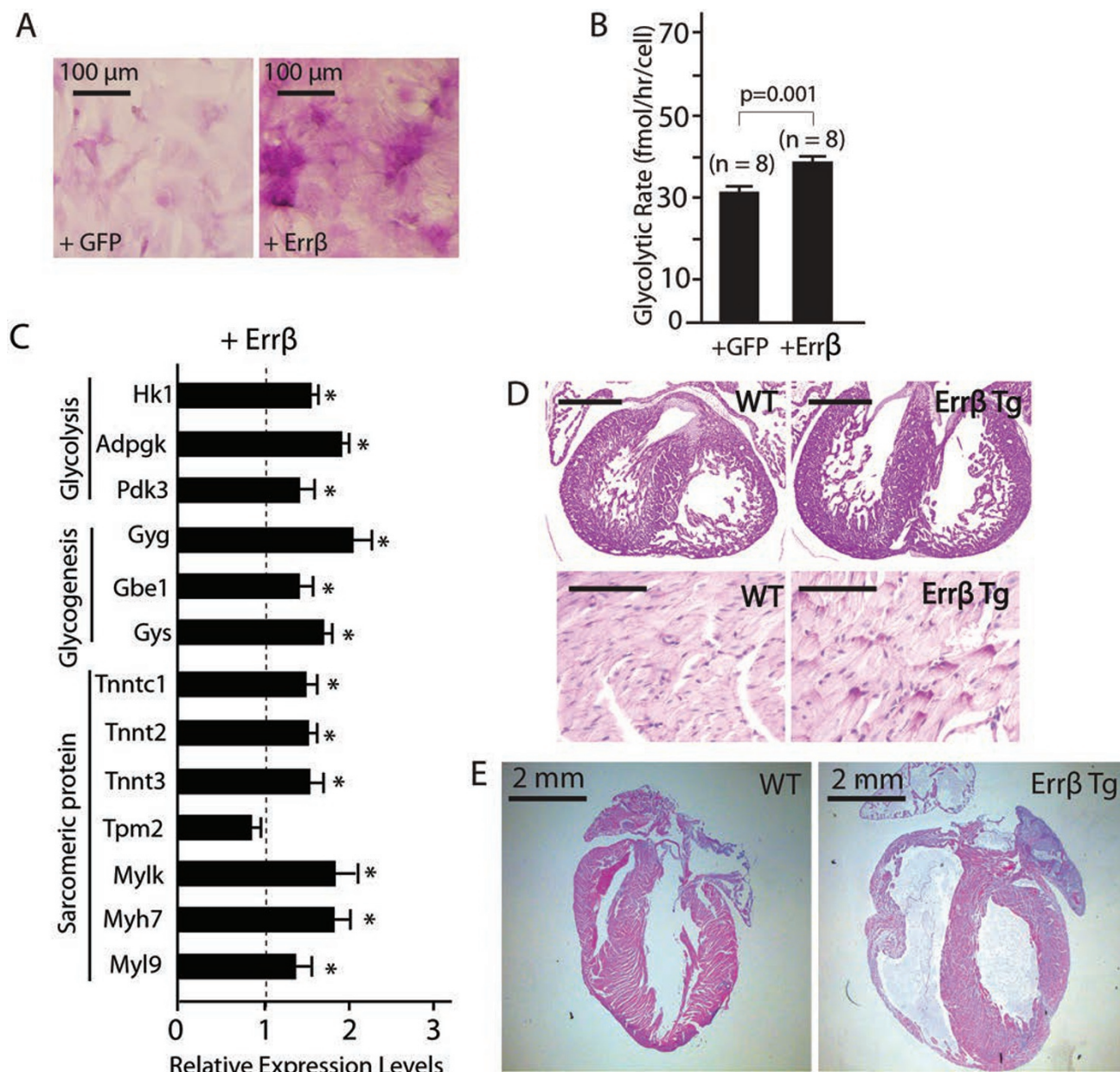

Figure 8 Errβ regulates the fetal gene program. **(A)** PAS staining of neonatal rat cardiomyocytes after overexpression of GFP and *Errβ*. **(B)** Glycolytic rate of neonatal rat cardiomyocytes after overexpression of GFP and *Errβ*. **(C)** *Errβ* was overexpressed in neonatal rat cardiomyocytes (*n* = 3). The expressions of those fetal genes were analyzed by qPCR (*n* = 3). *$P < 0.05$. **(D)** PAS staining of hearts from WT and *Errβ* Tg at E17.5 (top) or at postnatal stage (bottom). Scale bars, 100 μm (top) and 20 μm (bottom). **(E)** The H & E sections of the hearts from WT and *Errβ* Tg at 4 weeks of age. Tg: transgene.

firmed glycogen storage in *Errβ* transgenic mice (Figure 8D). Overexpression of *Errβ* in the heart led to cardiac dilation and sudden cardiac death around 3-4 weeks of age, which shares abnormalities seen in *miR-1 dKO* mice (Figure 8E and Supplementary information, Figure S10).

Discussion

In this study, we demonstrated that *miR-1*s orchestrate a genetic pathway involving *Errβ* that represses the cardiac fetal gene program in a multifaceted way.

A miR-1-directed genetic pathway involving Errβ critically represses the fetal gene program

The fetal heart is physiologically different from the adult heart in several ways: (1) Fetal cardiomyocytes rapidly divide, while adult cardiomyocytes grow almost exclusively in size. (2) The mechanical performance of the fetal heart is different from that of the adult heart [35]. (3) The fetal heart is mostly reliant on glycolysis as its energy source. In contrast, the adult heart utilizes long-chain fatty acids as the principal substrate for ATP production [36].

Adult cardiomyocytes in mammals were thought to terminally exit the cell cycle. Accumulating evidence now indicates that terminally differentiated cardiomyocytes can proliferate at a slow rate [37-39]. Therefore, enhancing cardiomyocyte proliferation may provide an alternative for cardiomyocyte regeneration and heart repair. We have seen numerous proliferating cardiomyocytes in neonates after loss of *miR-1*. Given the keen interest in cardiac regeneration [40-42], it will be interesting to exploit our findings to enhance adult cardiomyocyte proliferation.

We identified nuclear receptor gene *Errβ* as a direct target of *miR-1*, and they act together to regulate the expression of numerous fetal sarcomere-associated genes, such as *Tpm2*, *Myh7*, *Myl7*, *Myl9*, and *Acta2*, which normally decline in adulthood [43-47]. Continued expression of fetal sarcomeric proteins after birth can impair myocardial contraction and relaxation as exemplified by phenotypes associated with a mouse model with forced postnatal expression of Tpm2 [48]. Our work suggests that the increased expression of fetal sarcomeric proteins due to loss of *miR-1*s in postnatal heart alters the stoichiomeric composition of the sarcomere, decreasing myocardial performance and contributing to the development of DCM in *miR-1 dKO* mice.

Myocardial energy metabolism plays a key role in cardiac performance and heart diseases [49]. It is established that metabolic abnormalities such as mitochondrial syndromes can lead to cardiomyopathy [50, 51]. Recently, disease-causing mutations in the regulatory subunit of cardiac ATP-sensitive potassium (K_{ATP}) channels have been identified in patients with DCM [52]. Given that the glycolytic enzyme complex is associated with K_{ATP} channels [53], increased glycolysis, which can impair the ability of K_{ATP} to communicate between energetic status and membrane excitability, may at least partially contribute to the pathogenesis of DCM in *miR-1 dKO* mice. In addition, glycogen accumulation may also have detrimental effect on cardiac function in *miR-1 dKO* mice. Abnormally high glycogen stores have been found to account for clinical manifestations of cardiomyopathy as seen in familial hypertrophic cardiomyopathy and Pompe disease, although the precise mechanism by which accumulated glycogen causes cardiomyopathy remains unknown [13, 14]. We provide the first evidence that *Errβ* can stimulate glycogenesis. In the future, it will be interesting to explore whether they are involved in glycogen storage disease.

Our present work uncovers surprising multifaceted roles of *miR-1* in repressing the fetal gene program during the postnatal period. Nuclear receptor gene *Errβ* is identified as the direct target of *miR-1*, which can regulate glycolysis, glycogenesis, and fetal sarcomere-associated genes. DCM is the most common type of heart muscle disease in children, and it accounts for significant number of pediatric heart transplants. Compared with DCM in adult, the genetic causes of pediatric DCM remain relatively unknown and clinical treatment is not highly effective. Our data show that failure to properly suppress the fetal gene program can lead to DCM in newborns, which may provide an explanation for why pediatric DCM mostly occurs within first year after birth. If this holds true in humans, repressing the fetal gene program will be an effective strategy to treat certain types of pediatric DCM.

The miR-1s and miR-133as bicistron: key repressor for the cardiac fetal gene program

A comparison of the role of *miR-1* and *miR-133a* will be important as they reside in the same miRNA clusters. Deletion of both *miR-133a1* and *miR-133a2* causes lethal ventricular septal defect. Surviving *miR-133a* mutant mice develop DCM postnatally. In *miR-133a* dKO mice, transcript levels of *Acta2*, *Tagln*, *Cnn1*, *Cnn2*, and *Crp2* significantly increased, which are highly expressed in the fetal heart but not in the adult heart [4-8]. The increased expression of these genes is due to elevated level of Srf [34]. Srf, however, does not seem to participate in activating sarcomeric machinery after loss of *miR-1*s as the transcript level of Srf does not change in developing and postnatal hearts in *miR-1* dKO mice.

Recently, two groups reported *miR-1* dKO mice and

miR-1/*miR-133a* dKO mice [54, 55]. In both studies, positive selection cassettes (pGK-neo or lacZ-pGK-neo) were left in the *miR-1* loci. This complicates the interpretation of the results of these studies because it is known that pGK-neo cassettes can cause transcriptional interference [56]. Given the critical roles of *miR-133a* and *Mib1* in cardiac development and heart function [34, 57], that may explain why the phenotypes described for those mouse models differed from that observed in our study. For example, we and other group found increased cardiomyocyte proliferation after loss of *miR-1* or *miR-133a* [23, 34]; in contrast, cardiomyocyte proliferation was reported to be decreased in the *miR-1*/*miR-133a* dKO mice [55]. A comparison of the targeting strategies and mouse phenotypes is provided in Supplementary information, Figure S11.

miRNAs in the same cistron can exert synergic action [58]. Both *miR-1*s and *miR-133a* can repress fetal sarcomere genetic circuits and inhibit cell proliferation. While it remains to be determined whether *miR-133a* is also involved in glucose metabolism, our data clearly reveal the multifaceted role of *miR-1* in repressing the fetal cardiac gene program, i.e., cell proliferation, sarcomere-associated genes, glycolysis, and glycogenesis. Combined with the published *miR-1* and *miR-133a* null mouse models, an emerging common theme is that fetal genes such as *Anp*, *transgelin*, *Acta2*, *Tpm2*, *Mylk*, *Crp2* are upregulated when one or both of these miRNAs is absent. Thus, it is becoming clear that *miR-1*/*miR-133a* bicistron acts as a key repressor for the cardiac fetal gene program, playing a key role in driving cardiac maturation.

Materials and Methods

Generation of miR-1-1 and miR-1-2 conditional knockout mice and Errβ transgenic mice

Both *miR-1-1* and *miR-1-2* targeting vectors were constructed using BAC recombineering. In brief, Sv129 ES cells were electroporated with the targeting vector. Targeted ES cell colonies were identified by Southern blot. Two properly targeted ES cells were injected into C57BL6 blastocysts in the Mouse Genetics Shared Resource Facility at the Mount Sinai to generate high-percentage chimeras. *Errβ* was overexpressed under α-MHC promoter in *Errβ* transgenic mice. Mice with *miR-1* floxed allele were backcrossed at least six generations to a Sv129 isogenic background. All experiments with mice were performed according to protocols approved by the Institutional Animal Care and Use Committees of Icahn School of Medicine at Mount Sinai.

Massively parallel sequencing, real-time quantitative PCR, and RT-PCR analysis

Total RNAs were extracted from hearts at E15.5 or P2.5 using TRIzol Reagent. mRNAs were purified using a poly-A selection approach. Sequencing libraries were prepared according to a standard protocol. Samples were sequenced on the Illumina HiSeq

2000 platform in the Genomic Core at the Icahn School of Medicine at Mount Sinai. The single (100 bp) or paired-end reads (100 bp) were aligned to the mouse reference genome (NCBI Build 37/mm9) using TopHat program (Bowtie algorithm). Transcript assembles and identification of differentially expressed genes were achieved using Cufflinks package. To account for expression bias due to transcript length, each sample transcript expression was normalized by using cufflinks algorithm with a FDR of 0.05. Reads are available for download from the National Center for Biotechnology Information Sequence Read Archive under the accession number GSE45760.

qPCR was performed using StepOne plus (Applied Biosystems) per the manufacturer's protocol. Primer sequences are listed in Supplementary information, Table S6. 18S rRNA was used as an internal control. Semi-quantitative RT-PCR was done in the linear range of amplification.

Quantification of cardiomyocyte cell numbers, measurement of cell size, cell culture, and transfection assays

To quantify cell numbers, cardiomyocytes were isolated using an alkaline dissociation method as previously described [23]. Homogenous cell suspension was loaded onto a counting chamber. Cardiomyocytes in the counting chamber were distinguished from fibroblasts by cytoplasmic size and the presence of sarcomeres under phase contrast microscopy. The numbers of cardiomyocytes per mm^2 of the counting chamber were evaluated eight times per heart ($n = 3$).

To compare size of cardiomyocytes, heart sections were deparaffinized, rehydrated, and incubated with 100 μg/ml TRITC-labeled red wheat germ agglutinin for 1 h at room temperature. The cross-sectional area of left ventricular cardiomyocytes was measured using ImageJ. At least 100 cardiomyocytes were measured per field. Multiple sections obtained from four hearts per genotype were analyzed.

3′ UTR was subcloned into a pGL-TK vector and introduced into Cos cells with or without a plasmid containing *miR-1* or mutant *miR-1*. Luciferase assays were performed as described previously [24].

Neonatal rat ventricular myocytes were isolated by enzymatic dissociation of P1 or P2 neonatal Sprague-Dawley rat using the Neonatal Cardiomyocyte Isolation System (Worthington Biochemical Corp.) following the instruction manual. Neonatal rat ventricular myocytes were plated on gelatin-coated plates for 24 h, and then were infected with adenovirus expressing *miR-1*, *Errβ*, and GFP for 48 h with a multiplicity of infection (MOI) of 50. PAS staining, glycolysis assay, or total RNA isolation were performed 48 h after adenoviral transduction. High-titer recombinant human adenovirus type 5 expressing *miR-1* and *Errβ* were generated using the AdEasy™ Adenoviral Vector System (Agilent Technologies). A human Adenovirus Type 5 expressing GFP under the CMV promoter was used for control experiments.

Cell death analysis

TUNEL assay (In Situ Cell Death Detection Kit, Roche, Cat No: 11684809910) was used to detect apoptotic cells on paraffin sections. Evans Blue Dye (EBD) uptake was used to determine sarcolemmal integrity *in vivo*. Briefly, 1% EBD (wt/vol; 1 mg/0.1 ml PBS/10 g body weight) was administered by intraperitoneal injection at the right side of the peritoneal cavity, after which the animals were returned to their cage and allowed food and water

ad libitum. After 24 h, the mice were sacrificed, and hearts were excised, snap-frozen in liquid nitrogen and sectioned into cryosections of 7 μm thickness with a Leica cryostat. If there was necrosis, EBD was detected as red autofluorescence under a fluorescent microscope.

Energy metabolism

An enzymatic approach was used to measure glycolysis [32]. Briefly, neonatal hearts at P2.5 were dissected out and minced into small pieces, and cardiomyocytes were released by digestion with 229 U/ml collagenase type II (Worthington Biochemical). Separation of cardiomyocytes from fibroblasts was achieved by differential plating. Cardiomyocytes were grown on collagen-coated plate for 2 days. Cardiomyocytes were then pelleted and resuspended in Krebs buffer containing 1 mM glucose and 10 μCi/ml [5-^{3}H]-glucose for 1 h. Aliquots of each sample were added to 50 μl of 0.2 N HCl in 500-μl centrifuge tubes. These tubes were placed upright in scintillation vials containing 1 ml H_2O. The vials were sealed and permitted to equilibrate at 50 °C for 18-24 h. After the vapor-phase equilibration step, scintillation mixture was added to the vial for liquid scintillation counting. In the glycolytic pathway, ^3H_2O is formed from [5-^{3}H]-glucose at the enolase step, which can be used to calculate the amount of glucose. [5-^{3}H]-glucose and ^3H_2O standards were included to calculate the rate of conversion. Because the rate of glycolysis is correlated with the amount of cell number and time, glucose usage was calculated as follows:

(dpm sample-dpm zero time) × dilution factor of [5-^{3}H]-glucose × dilution factor of ^3H_2O for scintillation/specific activity (dpm/pmol glucose) × time (h) × number of cells × coefficient of equilibration.

Total glycogen content was measured by a spectrophotometic assay [59]. Briefly, glycogen was degraded to free glucose by Amyloglucosidase Reagent (Sigma-Aldrich A-7420). Glucose was converted to glucose-6-phosphate by hexokinase. In the presence of NAH, Glucose-6-phosphate dehydrogenase catalyzed glucose-6-phosphate into gluconic acid, resulting in the release of nicotinamide adenine dinucleotide phosphate (NADPH). The amount of NADPH was determined by the absorbance at 340 nm, which was used to calculate glucose amount by comparing to that from glucose standard solution. PAS staining was performed on paraffin sections following a standard protocol.

Oil Red O Staining was performed on frozen sections. Briefly, frozen sections at 7 μm thickness were immersed in the working solution of oil red O for 30 min, and then were washed with deionized water. Haematoxylin counterstaining was performed to visualize nuclei.

Transmission electron microscopy, fluorescence immunohistochemistry, picrosirius red staining, and western blot

For electron microscopy, the cardiac tissue was removed with a double-edged razor blade and dissected in a drop of glutaraldehyde fixative into tissue pieces that were no thicker than 2 mm. The tissues were then immediately immersion fixed in a solution of 3% glutaraldehyde in a 0.2 M sodium cacodylate, pH 7.2 buffer overnight. The tissue was then rinsed in a buffer solution of 0.2 M sodium cacodylate at pH 7.2, post-fixed with 1% osmium tetroxide for 1 h and again rinsed in the cacodylate buffer. The tissue was dehydrated in graded steps of ethanol and cleared in propylene

oxide and finally embedded in embed 812. After polymerization, 1 μl plastic sections were cut and stained with methylene blue and azure II and observed by light microscopy to choose representative cardiac tissue. The tissues were cut down and ultrathin sectioned and placed on 200 mesh copper grids, stained with uranyl acetate and lead citrate and observed with a Hitachi 7650 transmission electron microscope at 80 kV.

Confocal images were acquired with Leica SP5 DM in the microscope core at Mount Sinai using 40× objectives. Z spacing between slices was 1.3 μm.

Histological sectioning and hematoxylin and eosin staining were performed according to standard practices. Immunohistochemistry was performed on cryosections of 7 μm thickness.

Myocardial collagen was assessed by picrosirius red staining. Briefly, paraffin-embedded sections were stained in picrosirius red solution (Sigma: 365548) for 1 h after de-waxing. The sections were then dehydrated in absolute ethyl alcohol and examined with plane polarized light using Zeiss Axloplan 2.

Western blot was performed on heart tissues at P2.5 and P12. Source of antibodies and their dilutions were provided in Supplementary information, Table S7.

Noninvasive assessment of heart function

Transthoracic echocardiography was applied to the noninvasive serial assessment of cardiac function in mice using the Vevo 2100 ultrasound system (VisualSonics, Toronto, ON, Canada) at the In vivo Molecular Imaging SRF at Mount Sinai. Mice were lightly anesthetized with 1% isoflurane, and placed in dorsal recumbency on a heated 37 °C platform. A 30-MHz transducer was positioned over the chest in a parasternal long-axis view at the level of the great end-diastolic dimension. M-mode images were obtained for measurements. All data were analyzed using VevoStrain™ Analysis software.

Statistical analysis

Data were presented as mean ± standard error of the mean (SEM). Comparisons between groups were performed using unpaired two-tailed Student's *t*-test. The overlapping of genes and enrichment of miR-1 seed in 3′ UTR were assessed using the Fisher's exact test. The χ^2 test was used to test genotype frequency. The *P*-value < 0.05 was considered statistically significant.

Accession numbers

Massively parallel sequencing data was deposited to GEO with accession number GSE45760.

Acknowledgments

References

1   Rychik J. Fetal cardiovascular physiology. *Pediatr Cardiol* 2004; **25**:201-209.

2 Parker TG, Schneider MD. Growth factors, proto-oncogenes, and plasticity of the cardiac phenotype. *Annu Rev Physiol* 1991; **53**:179-200.

3 Schwartz K, Boheler KR, de la Bastie D, Lompre AM, Mercadier JJ. Switches in cardiac muscle gene expression as a result of pressure and volume overload. *Am J Physiol* 1992; **262**:R364-R369.

4 Ruzicka DL, Schwartz RJ. Sequential activation of alpha-actin genes during avian cardiogenesis: vascular smooth muscle alpha-actin gene transcripts mark the onset of cardiomyocyte differentiation. *J Cell Biol* 1988; **107**:2575-2586.

5 Li L, Miano JM, Cserjesi P, Olson EN. SM22 alpha, a marker of adult smooth muscle, is expressed in multiple myogenic lineages during embryogenesis. *Circ Res* 1996; **78**:188-195.

6 Samaha FF, Ip HS, Morrisey EE, *et al*. Developmental pattern of expression and genomic organization of the calponin-h1 gene. A contractile smooth muscle cell marker. *J Biol Chem* 1996; **271**:395-403.

7 Masuda H, Tanaka K, Takagi M, *et al*. Molecular cloning and characterization of human non-smooth muscle calponin. *J Biochem* 1996; **120**:415-424.

8 Jain MK, Kashiki S, Hsieh CM, *et al*. Embryonic expression suggests an important role for CRP2/SmLIM in the developing cardiovascular system. *Circ Res* 1998; **83**:980-985.

9 Arnold HH, Lohse P, Seidel U, Bober E. A novel human myosin alkali light chain is developmentally regulated. Expression in fetal cardiac and skeletal muscle and in adult atria. *Eur J Biochem* 1988; **178**:53-60.

10 Schaub MC, Hefti MA, Harder BA, Eppenberger HM. Various hypertrophic stimuli induce distinct phenotypes in cardiomyocytes. *J Mol Med (Berl)* 1997; **75**:901-920.

11 Depre C, Vanoverschelde JL, Taegtmeyer H. Glucose for the heart. *Circulation* 1999; **99**:578-588.

12 Pederson BA, Chen H, Schroeder JM, Shou W, DePaoli-Roach AA, Roach PJ. Abnormal cardiac development in the absence of heart glycogen. *Mol Cell Biol* 2004; **24**:7179-7187.

13 Arad M, Maron BJ, Gorham JM, *et al*. Glycogen storage diseases presenting as hypertrophic cardiomyopathy. *N Engl J Med* 2005; **352**:362-372.

14 Arad M, Benson DW, Perez-Atayde AR, *et al*. Constitutively active AMP kinase mutations cause glycogen storage disease mimicking hypertrophic cardiomyopathy. *J Clin Invest* 2002; **109**:357-362.

15 Desvergne B, Wahli W. Peroxisome proliferator-activated receptors: nuclear control of metabolism. *Endocr Rev* 1999; **20**:649-688.

16 Alaynick WA, Kondo RP, Xie W, *et al*. ERRgamma directs and maintains the transition to oxidative metabolism in the postnatal heart. *Cell Metab* 2007; **6**:13-24.

17 Tennessen JM, Baker KD, Lam G, Evans J, Thummel CS. The *Drosophila* estrogen-related receptor directs a metabolic switch that supports developmental growth. *Cell Metab* 2011; **13**:139-148.

18 Gan Z, Rumsey J, Hazen BC, *et al*. Nuclear receptor/microRNA circuitry links muscle fiber type to energy metabolism. *J Clin Invest* 2013; **123**:2564-2575.

19 Zhao Y, Srivastava D. A developmental view of microRNA function. *Trends Biochem Sci* 2007; **32**:189-197.

20 Espinoza-Lewis RA, Wang DZ. MicroRNAs in heart development. *Curr Top Dev Biol* 2012; **100**:279-317.

21 Wang J, Yang X. The function of miRNA in cardiac hypertrophy. *Cell Mol Life Sci* 2012; **69**:3561-3570.

22 Quiat D, Olson EN. MicroRNAs in cardiovascular disease: from pathogenesis to prevention and treatment. *J Clin Invest* 2013; **123**:11-18.

23 Zhao Y, Ransom JF, Li A, *et al*. Dysregulation of cardiogenesis, cardiac conduction, and cell cycle in mice lacking *miRNA-1-2*. *Cell* 2007; **129**:303-317.

24 Zhao Y, Samal E, Srivastava D. Serum response factor regulates a muscle-specific microRNA that targets *Hand2* during cardiogenesis. *Nature* 2005; **436**:214-220.

25 Yang B, Lin H, Xiao J, *et al*. The muscle-specific microRNA *miR-1* regulates cardiac arrhythmogenic potential by targeting *GJA1* and *KCNJ2*. *Nat Med* 2007; **13**:486-491.

26 Shan H, Li X, Pan Z, *et al*. Tanshinone IIA protects against sudden cardiac death induced by lethal arrhythmias via repression of microRNA-1. *Br J Pharmacol* 2009; **158**:1227-1235.

27 Girmatsion Z, Biliczki P, Bonauer A, *et al*. Changes in microRNA-1 expression and I_{K1} up-regulation in human atrial fibrillation. *Heart Rhythm* 2009; **6**:1802-1809.

28 Ikeda S, He A, Kong SW, *et al*. MicroRNA-1 negatively regulates expression of the hypertrophy-associated calmodulin and *Mef2a* genes. *Mol Cell Biol* 2009; **29**:2193-2204.

29 Chen JF, Mandel EM, Thomson JM, *et al*. The role of microRNA-1 and microRNA-133 in skeletal muscle proliferation and differentiation. *Nat Genet* 2006; **38**:228-233.

30 Wei Y, Mizzen CA, Cook RG, Gorovsky MA, Allis CD. Phosphorylation of histone H3 at serine 10 is correlated with chromosome condensation during mitosis and meiosis in *Tetrahymena*. *Proc Natl Acad Sci USA* 1998; **95**:7480-7484.

31 Narula J, Haider N, Virmani R, *et al*. Apoptosis in myocytes in end-stage heart failure. *N Engl J Med* 1996; **335**:1182-1189.

32 Ashcroft SJ, Weerasinghe LC, Bassett JM, Randle PJ. The pentose cycle and insulin release in mouse pancreatic islets. *Biochem J* 1972; **126**:525-532.

33 Wang D, Chang PS, Wang Z, *et al*. Activation of cardiac gene expression by myocardin, a transcriptional cofactor for serum response factor. *Cell* 2001; **105**:851-862.

34 Liu N, Bezprozvannaya S, Williams AH, *et al*. microRNA-133a regulates cardiomyocyte proliferation and suppresses smooth muscle gene expression in the heart. *Genes Dev* 2008; **22**:3242-3254.

35 Friedman WF. The intrinsic physiologic properties of the developing heart. *Prog Cardiovasc Dis* 1972; **15**:87-111.

36 Lopaschuk GD, Jaswal JS. Energy metabolic phenotype of the cardiomyocyte during development, differentiation, and postnatal maturation. *J Cardiovasc Pharmacol* 2010; **56**:130-140.

37 Senyo SE, Steinhauser ML, Pizzimenti CL, *et al*. Mammalian heart renewal by pre-existing cardiomyocytes. *Nature* 2013; **493**:433-436.

38 Parmacek MS, Epstein JA. Cardiomyocyte renewal. *N Engl J Med* 2009; **361**:86-88.

39 Bergmann O, Bhardwaj RD, Bernard S, *et al*. Evidence for cardiomyocyte renewal in humans. *Science* 2009; **324**:98-102.

40 Yi BA, Wernet O, Chien KR. Pregenerative medicine: developmental paradigms in the biology of cardiovascular regeneration. *J Clin Invest* 2010; **120**:20-28.

41 Bu L, Jiang X, Martin-Puig S, *et al*. Human ISL1 heart progenitors generate diverse multipotent cardiovascular cell lineages. *Nature* 2009; **460**:113-117.

42 Ieda M, Fu JD, Delgado-Olguin P, *et al*. Direct reprogramming of fibroblasts into functional cardiomyocytes by defined factors. *Cell* 2010; **142**:375-386.

43 Muthuchamy M, Pajak L, Howles P, Doetschman T, Wieczorek DF. Developmental analysis of *tropomyosin* gene expression in embryonic stem cells and mouse embryos. *Mol Cell Biol* 1993; **13**:3311-3323.

44 Muthuchamy M, Boivin GP, Grupp IL, Wieczorek DF. *Beta-tropomyosin* overexpression induces severe cardiac abnormalities. *J Mol Cell Cardiol* 1998; **30**:1545-1557.

45 Morkin E. Control of cardiac myosin heavy chain gene expression. *Microsc Res Tech* 2000; **50**:522-531.

46 Schildmeyer LA, Braun R, Taffet G, *et al*. Impaired vascular contractility and blood pressure homeostasis in the smooth muscle alpha-actin null mouse. *FASEB J* 2000; **14**:2213-2220.

47 Birukov KG, Schavocky JP, Shirinsky VP, Chibalina MV, Van Eldik LJ, Watterson DM. Organization of the genetic locus for chicken myosin light chain kinase is complex: multiple proteins are encoded and exhibit differential expression and localization. *J Cell Biochem* 1998; **70**:402-413.

48 Palmiter KA, Kitada Y, Muthuchamy M, Wieczorek DF, Solaro RJ. Exchange of beta- for alpha-tropomyosin in hearts of transgenic mice induces changes in thin filament response to Ca^{2+}, strong cross-bridge binding, and protein phosphorylation. *J Biol Chem* 1996; **271**:11611-11614.

49 Stanley WC, Recchia FA, Lopaschuk GD. Myocardial substrate metabolism in the normal and failing heart. *Physiol Rev* 2005; **85**:1093-1129.

50 Ahmad F, Seidman JG, Seidman CE. The genetic basis for cardiac remodeling. *Annu Rev Genomics Hum Genet* 2005; **6**:185-216.

51 Kelly DP, Strauss AW. Inherited cardiomyopathies. *N Engl J Med* 1994; **330**:913-919.

52 Bienengraeber M, Olson TM, Selivanov VA, *et al*. ABCC9 mutations identified in human dilated cardiomyopathy disrupt catalytic K_{ATP} channel gating. *Nat Genet* 2004; **36**:382-387.

53 Weiss JN, Lamp ST. Glycolysis preferentially inhibits ATP-sensitive K^+ channels in isolated guinea pig cardiac myocytes. *Science* 1987; **238**:67-69.

54 Heidersbach A, Saxby C, Carver-Moore K, *et al*. microRNA-1 regulates sarcomere formation and suppresses smooth muscle gene expression in the mammalian heart. *Elife* 2013; **2**:e01323.

55 Wystub K, Besser J, Bachmann A, Boettger T, Braun T. *miR-1/133a* clusters cooperatively specify the cardiomyogenic lineage by adjustment of myocardin levels during embryonic heart development. *PLoS Genet* 2013; **9**:e1003793.

56 Ema M, Takahashi S, Rossant J. Deletion of the selection cassette, but not cis-acting elements, in targeted *Flk1-lacZ* allele reveals *Flk1* expression in multipotent mesodermal progenitors. *Blood* 2006; **107**:111-117.

57 Luxan G, Casanova JC, Martinez-Poveda B, *et al*. Mutations in the NOTCH pathway regulator *MIB1* cause left ventricular noncompaction cardiomyopathy. *Nat Med* 2013; **19**:193-201.

58 Kim YK, Yu J, Han TS, *et al*. Functional links between clustered microRNAs: suppression of cell-cycle inhibitors by microRNA clusters in gastric cancer. *Nucleic Acids Res* 2009; **37**:1672-1681.

59 Wende AR, Schaeffer PJ, Parker GJ, *et al*. A role for the transcriptional coactivator PGC-1alpha in muscle refueling. *J Biol Chem* 2007; **282**:36642-36651.

(**Supplementary information** is linked to the online version of the paper on the *Cell Research* website.)